

Intrinsic circular polarization in centrosymmetric stacks of transition-metal dichalcogenides

Qihang Liu^{*}, Xiuwen Zhang, and Alex Zunger^{*}

University of Colorado, Boulder, CO 80309, USA

^{*}E-mail: qihang.liu85@gmail.com; alex.zunger@gmail.com.

Abstract

The circular polarization (CP) that the photoluminescence inherits from the excitation source in n monolayers of transition-metal dichalcogenides $(MX_2)_n$ has been previously explained as a special feature of *odd* values of n , where the inversion symmetry is absent. This “valley polarization” effect results from the fact that in the absence of inversion, charge carriers in different band valleys could be selectively excited by different circular polarized light. Such restriction to non-centrosymmetric systems poses a limitation on the material selection for achieving CP. Although several experiments observed CP in centrosymmetric MX_2 systems e.g., for bilayer in MX_2 , they were dismissed as being due to some extrinsic sample irregularities. Here we show that also for $n = \text{even}$ where inversion symmetry is present and valley polarization physics is strictly absent, such intrinsic selectivity in CP is to be expected on the basis of fundamental spin-orbit physics. First-principles calculations of CP predict significant polarization for $n = 2$ bilayers: from 69% in MoS_2 to 93% in WS_2 . This realization could broaden the range of materials to be considered as CP sources.

The quest for a system manifesting a single type of circular polarized light – left-handed (LH, or σ_+) or right-handed (RH, or σ_-) has been motivated by its promising application in fields such as spin-Hall effect and quantum computation [1-6]. The magnitude of the effect is conveniently measured by circular polarization (CP), i.e., the anisotropy of circular polarized luminescence [7]

$$\rho = \frac{I(\sigma_+) - I(\sigma_-)}{I(\sigma_+) + I(\sigma_-)}, \quad (1)$$

where $I(\sigma_+)$ and $I(\sigma_-)$ denotes the intensity of the LH and RH polarized luminescence, respectively. Generating significant ρ requires both that the excited quantum entities have intrinsically pure LH or RH symmetries, and that the relaxation processes following excitation do not mix RH with LH states. One approach to creation of CP is the utilization of *spin-orbit-induced CP* [6] in which spin-orbit coupling (SOC) in low-symmetry bulk solids creates spin splitting (the Dresselhaus [8] and Rashba [9] effects), leading to spin-sensitive absorption and thus polarized luminescence. This is limited to non-centrosymmetric systems. Another approach to achieving large ρ is the direct creation of *valley-selective CP* [10]. Here absorption selects the wavefunction character that can couple with the circular polarized light, and SOC is not needed to produce the effect. An example is $n = \text{odd}$ monolayers of 2H-stacking transition-metal dichalcogenides $(MX_2)_n$ (with M : Mo, W; and X : S, Se), having two valleys K and $-K$ with equal energies located at the corners of their hexagonal Brillouin zone. For a single monolayer, the valence band maximum (VBM) occurs at these wavevectors and the corresponding wavefunctions $\psi_v^{(n=1)}(K) = \chi_+$ and $\psi_v^{(n=1)}(-K) = \chi_-$ have pure LH or RH characters, respectively. As a result, σ_+ excitation can excite the valence electrons at the K valley but no electrons at the $-K$ valley, while σ_- can only excite valence electrons at the $-K$ valley but none of those at the K valley. This valley selectivity is also limited to non-centrosymmetric systems ($n = \text{odd}$ stacks). Such valley-contrasting CP (“valley polarization”) leads to valleytronics, a parallel concept of spintronics, with the emergence of interesting phenomena such as valley-Hall effect [11, 12]. However, the limitation to non-centrosymmetric systems both in the spin-orbit induced CP and in the valleytronics-induced CP poses a restriction on material selection for achieving CP.

Surprisingly, highly selective (up to $\rho = 80\%$) CP has been observed in emission also in $n = 2$ $(MX_2)_n$ (bilayer) which has inversion symmetry [7, 13-16]. Since this goes against the generally accepted expectation that valley-induced CP should be intrinsically absent in centrosymmetric (such as even n) materials, various *extrinsic* scenarios were offered to rationalize this unusual observation, such as substrate charging, low-quality sample, and heating effects, etc. [7, 15, 16].

Recently, Gong et al. [17] discussed the magnetoelectric effects of bilayer MX_2 using $\mathbf{k} \cdot \mathbf{p}$ and tight-binding method. They have argued that because the interlayer coupling is weak, bilayers will inherit most of the spin-valley physics of monolayers, named “spin-layer locking”. In this Letter, we focus instead on spin-orbit physics as local effect, building on the recent realization [18] that SOC-induced spin polarization can exist not only when inversion symmetry is absent (the ordinary Dresselhaus or Rashba effects), but also in systems where inversion symmetry is present (i.e., globally centrosymmetric systems) while its individual sectors (e.g., monolayers) lack inversion. We show that such “hidden spin polarization” can lead to circular polarization in emission for $n = \text{even}$ values of $(MX_2)_n$. This is illustrated in Fig. 1 showing our first-principles calculated ρ for resonant excitation at K and $-\text{K}$ valley as a function of the number of monolayers n in $(MX_2)_n$, reaching asymptotically the bulk value for large n . We see that the CP decreases monotonically with increasing n and the results of n lie on one curve without odd-even oscillations, in contrast with the expectation based on valley symmetries [10, 15, 16]. Our “hidden spin polarization” mechanism provides a specific physical realization to the general principle of weak interlayer coupling proposed by Gong et al. By recognizing that it is the spin-orbit physics that can induce CP and that it is no longer limited to rather rare low-symmetry structures this could broaden the range of materials to be considered as CP spintronic sources.

Spin-orbit induced local spin polarization S in each monolayer within the bilayer $(MX_2)_2$ system. This intrinsic CP in centrosymmetric systems originating from “hidden spin polarization” can be illustrated for bilayer $n = 2$ in $(MX_2)_n$, where two inversion-asymmetric individual MX_2 layers α and β (“sectors” in general) carry opposite local spin polarization. In bilayer MX_2 , a monolayer MX_2 named β is introduced to form inversion partner with layer α . The corresponding energy bands must be spin-degenerate due to the

combination of inversion symmetry and time-reversal symmetry. However, such global k -space compensation of spins does not occur in a point-by-point fashion in real space, i.e., on each MX_2 layer. Using density functional theory (DFT) calculation implemented by VASP [19] with projected augmented wave (PAW) pseudopotential [20], we can project the two-fold degenerate wavefunction $|\phi\rangle$ with plane-wave expansion on the spin and orbital basis (spherical harmonics) of each atomic site. For K valley of the top valence band (V1),

$$\begin{aligned}\psi_v^{n=2}(K, \uparrow) &= \sum_{l,m,i} C_{l,m,i,\uparrow} |l, m\rangle_i \otimes |\uparrow\rangle, \\ \psi_v^{n=2}(K, \downarrow) &= \sum_{l,m,i} C_{l,m,i,\downarrow} |l, m\rangle_i \otimes |\downarrow\rangle,\end{aligned}\tag{2}$$

with the expansion coefficient

$$C_{i,l,m,m_z} = \langle \phi | (s_z \otimes |l, m\rangle_i \langle l, m|) | \phi \rangle \tag{3}$$

where $|l, m\rangle_i$ is the orbital angular momentum eigenstate of the i th atomic site, and $s_z = \frac{\hbar}{2} \sigma_z$ is the spin operator. Note that s_z is a good quantum number with two spin eigenstates $|\uparrow\rangle$ and $|\downarrow\rangle$ ($m_z = \pm 1$). By summing $C_{i,l,m,\eta}$ separately for layer α and for layer β (each containing 3 atomic sites in the unit cell), we find that for K valley of V1 in bilayers of MoS_2 , MoSe_2 , WS_2 , and WSe_2 the spin polarization $S = \sum_{l,m,m_z,i \in \alpha} C_{i,l,m,m_z}$ localized on layer α is 0.83, 0.90, 0.97 and 0.95 (out-of plane, in the unit of $\frac{\hbar}{2}$) respectively, and the local spin polarization on layer β has exactly the same magnitude but opposite direction. Thus, despite global inversion of the $n = 2$ structure, each individual layer experiences a nonzero local spin polarization S in real space, “hidden” by the presence of the counterpart on the other layer. We will next show that in such even-layer stacks of $(MX_2)_n$ hidden spin polarization induce CP as an intrinsic part of the fundamental physics even without any sample irregularities.

Photoluminescence process leading to circular polarization. To calculate CP of Eq. (1) that involves *emission* experiment, we need a model of what happens to the photo excited carriers before emission. Taking bilayer MX_2 as an example, we will next consider the absorption, relaxation and emission process, as illustrated in Fig. 2. The splitting between the top two valence bands V1 and V2 at K and $-\text{K}$ is due to SOC-induced spin splitting and the interlayer coupling. Here we consider resonant excitation

(the incident photon energy equals to the direct band gap at K or $-K$), in which only V1 is of interest.

Interband absorption is described by the up arrow indicated as ① in Fig. 2(a). It involves by promoting an electron from a valence band eigenstate of Eq. (2) into a conduction band eigenstate, evaluated by the transition matrix element $\mathcal{P}_{\pm} = \langle \psi_c | p_x \pm ip_y | \psi_v \rangle$, where \mathbf{p} is the momentum operator. By calculating the transition matrix element for circular polarized light, say σ_+ , we find that unlike the case of one monolayer in which absorption is valley contrasting, in bilayer MX_2 the K and $-K$ valley have the same absorption, consistent with the presence of global inversion symmetry [10]. However, as shown above, the two degenerate spin states shown in Eq. (2) have different non-zero absorption magnitude, leading to a net spin of the excited electrons. To interpret this effect and its impact on CP, we reconsider the valence band eigenstates of the bilayer system in Eq. (2) expanded in terms of single monolayer eigenstates, $\psi_v^{(n=1)}(K) = \chi_+$ and $\psi_v^{(n=1)}(-K) = \chi_-$ having pure LH or RH characters, respectively. We approximate the wavefunction of bilayer MX_2 at K valley as an expansion in terms of the α layer ($\chi_+^{(\alpha)}$) and $-K$ valley of β layer ($\chi_-^{(\beta)}$) eigenstates, written as

$$\begin{aligned}\psi_v^{(n=2)}(K, \uparrow) &= (C_{\alpha, \uparrow} \chi_+^{(\alpha)} + C_{\beta, \uparrow} \chi_-^{(\beta)}) \otimes |\uparrow\rangle, \\ \psi_v^{(n=2)}(K, \downarrow) &= (C_{\alpha, \downarrow} \chi_+^{(\alpha)} + C_{\beta, \downarrow} \chi_-^{(\beta)}) \otimes |\downarrow\rangle,\end{aligned}\quad (4)$$

where $C_{\alpha(\beta), m_z}^2 = \sum_{l, m, m_z, i \in \alpha(\beta)} C_{i, l, m, m_z}^2$, and $C_{\alpha, \uparrow} = C_{\beta, \downarrow} = C_{maj}$, $C_{\beta, \uparrow} = C_{\alpha, \downarrow} = C_{min}$. Subscript $+$ ($-$) denotes pure LH (RH) wavefunction component, while superscripts denote real space monolayer α or β . The wavefunctions of V1 at $-K$ valley is just related to those at K valley by time reversal

$$\begin{aligned}\psi_v^{(n=2)}(-K, \uparrow) &= (C_{maj} \chi_+^{(\beta)} + C_{min} \chi_-^{(\alpha)}) \otimes |\uparrow\rangle, \\ \psi_v^{(n=2)}(-K, \downarrow) &= (C_{min} \chi_+^{(\beta)} + C_{maj} \chi_-^{(\alpha)}) \otimes |\downarrow\rangle.\end{aligned}\quad (5)$$

Here C_{maj} and C_{min} denote the majority (maj) and minority (min) component for each valence spin state. We have tested the approximation of expanding $n = 2$ just by the two $n = 1$ eigenstates by calculating the ratio of transition matrix elements $\mathcal{P}_+(K, \uparrow)/\mathcal{P}_+(K, \downarrow)$ of the corresponding spin states with initial plane-wave expansion via first-principles

calculation, and find it in good agreement with C_{maj}^2/C_{min}^2 from Eq. (4) and (5), indicating the validity of our wavefunction decomposition onto the monolayer basis.

Unlike the case of one monolayer in which the VBM states have pure LH or RH components (χ_+ and χ_-), the four valence states of bilayer MX_2 , described by Eq. (4) and (5), have both χ_+ and χ_- components. Therefore, for σ_+ resonant excitation only the electrons with $\chi_+^{(\alpha)}$ character at the K valley and the electrons with $\chi_+^{(\beta)}$ character at the $-K$ valley are excited (χ_- components have no contribution to the transition matrix element), as shown in Fig. 2 by step ①. Note that for $\psi_v(K, \uparrow)$ and $\psi_v(-K, \uparrow)$ eigenstates [Fig. 2(b) and (d)], the excited component is the majority term (proportional to C_{maj}^2) with up-spin $|\uparrow\rangle$, while for $\psi_v(K, \downarrow)$ and $\psi_v(-K, \downarrow)$ states [Fig. 2(a) and (c)], the excited component is the minority term (proportional to C_{min}^2) with down-spin $|\downarrow\rangle$. As a result, the excited electrons have a net up-spin that equals to the local spin polarization on each layer at K or $-K$ valley (absolute value) derived from Eq. (4) and (5), $S = \frac{C_{maj}^2 - C_{min}^2}{C_{maj}^2 + C_{min}^2}$, creating simultaneously equivalent holes with the same net spin.

Following excitation, relaxation mechanisms might redistribute the photogenerated LH and RH holes, thereby reducing the polarization anisotropy ρ . The observed ρ for monolayer MoS_2 has been as large as 100% [7], suggesting ineffective mixture of photogenerated LH and RH holes caused by intervalley relaxation and thus excellent retention of the valley-contrasting circular absorption. In bilayer MX_2 , the dominated relaxation route considered here is illustrated by the green arrow labeled step ② in Fig. 2(a). For the σ_+ excitation, all of the promoted electrons have χ_+ character, leaving the excited state with a different LH/RH ratio compared with the ground state. Consequently, the LH and RH components tends to redistribute within the same valence eigenstate to retain the ground state ($\chi_- \rightarrow \chi_+$). Such intrastate relaxation could happen much faster than the electron recombination because of the imbalance excitation between χ_+ and χ_- components and the lack of effective barrier to suppress the spin-conserved relaxation. Three kinds of other relaxation channels that could mix LH and RH components and thus affect ρ are also considered. We assume the relaxation time with spin flip much slower,

while the relaxation time with spin conserving much faster, than the electron recombination time, with the details listed in Supplementary Materials [21].

As indicated by red and blue curled arrows (step ③), the radiative recombination fills the holes with χ_+ and χ_- characters of valence band, leading to σ_+ and σ_- luminescence, respectively. In Fig. 2(a) and (c), the excited χ_+ component is majority, so the total emission is larger than that in Fig. 2(b) and (d), in which excited χ_+ component is minority. In addition, the magnitude of σ_+ and σ_- emission in each state also reflects the comparison of χ_+ and χ_- components. Based on the description of the relaxation and emission processes following absorption, and the assumptions mentioned above, an expression for the total CP from Eq. (1) is thus derived [21]

$$\rho = \left(\frac{c_{maj}^2 - c_{min}^2}{c_{maj}^2 + c_{min}^2} \right)^2. \quad (6)$$

Similarly, we can get exactly opposite ρ by using σ_- resonant excitation (see Fig. S1 [21]). From Eq. (6) we find that the polarization anisotropy ρ is closely related to S : there is no intrinsic CP unless there is local spin on each MX_2 layer. Generally, if a centrosymmetric material has local spin polarization on each inversion-asymmetric sector, we can find non-zero CP following excitation of circular polarized light, as all the MX_2 bilayers shown in Fig. 1.

Progression of CP from $n = 1$ to bulk MX_2 . From the above discussion we note that the CP of bilayer MX_2 is directly related to the spin polarization localized on each layer, rather than the global inversion symmetry. This dependence provides us the route to evaluate CP for all $(MX_2)_n$ stacks by directly calculating the ratio of LH/RH components of the valence band wavefunctions expanded by monolayer basis. For 2H- MX_2 stacking pattern, the K (–K) valley of each monolayer in $(MX_2)_n$ has pure LH or RH component alternatively, depending on the odd-even parity of the layer index. When $n > 1$, The band edges of $(MX_2)_n$ at K and –K valley, no matter degenerate or non-degenerate, have no longer a certain helicity, but a mixture of LH and RH characters from different layers, leading to the reduction of CP away from the case of monolayer. If the orbital part of (one of) the valence band wavefunction at K or –K valley of $(MX_2)_n$ is written as

$$\psi_v = c_1\chi_+^{(1)} + c_2\chi_-^{(2)} + c_3\chi_+^{(3)} + \cdots + c_n\chi_{+/-}^{(n)}, \quad (7)$$

where C_i ($i = 1, 2, \dots, n$) is the coefficient of LH or RH component from the i th layer, we can thus obtain the corresponding theoretical circular polarization by resonant excitation

$$\rho = \left(\frac{\sum_n (-1)^{n-1} C_n^2}{\sum_n C_n^2} \right)^2. \quad (8)$$

Note that although spin part is not included to calculate the CP, it plays a crucial role for the spin-conserving intrastate relaxation and the prevention of spin-flip relaxation. The CP of four $(MX_2)_n$ materials as a function of the layer number n is shown in Fig. 1. Contrasting with the conventional understanding that the CP should oscillate with odd-even layers due to the absence or presence of inversion symmetry, we found decreasing polarization ratio with n . All of $(WX_2)_n$ stacks have higher ρ than that of $(MoX_2)_n$ due to the larger SOC of W atom. All the CP curves reveal an asymptotic behavior to the bulk value. This is because starting from $n = 1$ in which the valence states have pure LH or RH component, the ratio between LH/RH tends to saturate as n increases.

Such trend is confirmed by a very recent experiment on few-layer 2H-MoS₂ [22], which also exhibits a decreasing dependence on layer number with saturation, indicating a good agreement with our prediction except for the starting point of CP in monolayer (about 58%, possibly because of the sample quality). Some other experiments also detected nonzero polarized luminescence ρ_{exp} of MX_2 bilayers, but lower than our calculated theoretical limit (e.g., 14% lower for bilayer WS₂ [14]). We list the possible reasons in the Supplementary Materials [21]. Furthermore, because of the local spin on each MX_2 layer, the CP range from 37% (MoS₂) to 83% (WS₂) even for 2H-stacking *bulk* MX_2 crystal. Recently, the “hidden spin polarization” effect in bulk WSe₂ has been observed experimentally by spin- and angle-resolved photoemission spectroscopy (SR-ARPES) [23], revealing large layer-dependent local spin polarization. Therefore, we expect the intrinsic CP in centrosymmetric bulk MX_2 to be realized by upcoming measurements.

Dependence of ρ on the interlayer distance and material design of larger CP: The dependence of ρ on the interlayer distance for different bilayer MX_2 compounds is shown in Fig. 3. The curves clearly exhibit that the intrinsic CP is enhanced as the interlayer separation increases, which could be achieved by tensile strain along stacking direction or within the two-dimensional (2D) plane [24]. At the equilibrium separation (experimental

values indicated by solid symbols), our calculated CP is 69% for MoS₂, 81% for MoSe₂, 90% for WSe₂, and 93% for WS₂ [25]. We further note that for the same interlayer distance, the CP of WX₂ is larger than that of MoX₂. Furthermore, when the interlayer distance of the MX₂ bilayer exceeds 4 Å, the coupling between α and β layer becomes negligible, implying perfect local spin polarization. As a result, the CP approaches monolayer limit $\rho = 1$ when the interlayer distance is large enough.

Using the understanding of hidden spin polarization, we next design a heterostructure with better CP performance by intercalating a 2D wide-gap semiconductor BN as inert medium into bilayer MoSe₂. The latter compound has the lowest ρ for a fixed interlayer distance, as shown in Fig. 3; and the ratio of lattice constant between MoSe₂ and BN is 4:3 with the mismatch less than 1%. Figure S2 shows our calculated band structure of centrosymmetric MoSe₂/BN/BN/MoSe₂ heterostructure with a supercell containing 3×3 MoSe₂ and 4×4 BN within perfect planar alignment, and that of monolayer MoSe₂ with 3×3 periodicity for comparison [21]. After structure optimization with the van der Waals correction considered by a dispersion-corrected PBE-D2 method [26], we find that BN layer and the adjacent S layer are still flat with the interlayer distance 3.56 Å, indicating weak coupling between the two kinds of 2D materials. The band structure of the heterostructure is nearly the same as that of monolayer MoSe₂ in 3×3 supercell, except some BN character far from the Fermi level. By analyzing the wavefunction of the band edges we find that the heterostructure performs as two non-interacting MoSe₂ monolayers, with each layer carrying opposite local spin polarization $S \approx \pm 1$. In addition, such heterostructure could also avoid the indirect-bandgap problem of bilayer MoSe₂ and thus make excitons stable at K valley to reduce the loss of ρ [21]. Similar heterostructures have been synthesized by mechanically stacking graphene, h-BN and MoS₂ in order on the substrate [27]. We believe that such sandwiched structures as the proposed MoSe₂/BN heterostructure, having both optimized polarization anisotropy $\rho \approx 1$ and direct bandgap, are good platforms to realize intrinsic CP in a centrosymmetric system by the current synthesis technology [28].

In summary, by using first-principle calculations, we demystify the occurrence of intrinsic CP in centrosymmetric layer stacks made of individually non-centrosymmetric layers, such as $n = \text{even}$ (MX₂)_n. The intrinsic CP decreases monotonically with

increasing n , in sharp contrast with the expectation of odd-even oscillations based on valley symmetries. Such polarization anisotropy results from hidden spin polarization that is localized on each MX_2 layer. The local spin leads to imbalance absorption of electrons with different spin states, and thus ensures a large CP to be 69% (bilayer MoS_2) - 93% (bilayer WS_2) after relaxation and retention. Our finding is expected to broaden the material selection that is currently limited to non-centrosymmetric systems for achieving CP and related phenomena, and provide new possibility for the manipulation of spin in the field of spintronics and optoelectronics.

Acknowledgements

We are grateful for the good discussions with Yu Ye from UC Berkeley, Yang Song from Rochester University and helpful codes for the calculation of transition matrix elements from Kanber Lam, Northwestern University. This work was supported by NSF Grant No. DMREF-13-34170. This work used the Extreme Science and Engineering Discovery Environment (XSEDE), which is supported by National Science Foundation grant number ACI-1053575.

Reference

- [1] A. Crepaldi *et al.*, Phys. Rev. B **89**, 125408 (2014).
- [2] T. D. Nguyen, E. Ehrenfreund, and Z. V. Vardeny, Science **337**, 204 (2012).
- [3] V. L. Korenev, I. A. Akimov, S. V. Zaitsev, V. F. Sapega, L. Langer, D. R. Yakovlev, Y. A. Danilov, and M. Bayer, Nat Commun **3**, 959 (2012).
- [4] M. Ghali, K. Ohtani, Y. Ohno, and H. Ohno, Nat. Commun. **3**, 661 (2012).
- [5] J. Wunderlich, B. Kaestner, J. Sinova, and T. Jungwirth, Phys. Rev. Lett. **94**, 047204 (2005).
- [6] F. Meier and B. P. Zakharchenya, *Optical Orientation* (Elsevier Science Publishers B.V., 1984).
- [7] K. F. Mak, K. He, J. Shan, and T. F. Heinz, Nat. Nanotech. **7**, 494 (2012).
- [8] G. Dresselhaus, Phys. Rev. **100**, 580 (1955).
- [9] E. I. Rashba, Soviet Physics-Solid State **2**, 1109 (1960).
- [10] W. Yao, D. Xiao, and Q. Niu, Phys. Rev. B **77**, 235406 (2008).
- [11] D. Xiao, G.-B. Liu, W. Feng, X. Xu, and W. Yao, Phys. Rev. Lett. **108**, 196802 (2012).
- [12] X. Xu, W. Yao, D. Xiao, and T. F. Heinz, Nat. Phys. **10**, 343 (2014).
- [13] A. M. Jones, H. Yu, J. S. Ross, P. Klement, N. J. Ghimire, J. Yan, D. G. Mandrus, W. Yao, and X. Xu, Nat. Phys. **10**, 130 (2014).

- [14] H. Z. Bairen Zhu, Junfeng Dai, Zhirui Gong, Xiaodong Cui, arXiv:1403.6224 (2014).
- [15] S. Wu *et al.*, Nat. Phys. **9**, 149 (2013).
- [16] H. Zeng, J. Dai, W. Yao, D. Xiao, and X. Cui, Nat. Nanotech. **7**, 490 (2012).
- [17] Z. Gong, G.-B. Liu, H. Yu, D. Xiao, X. Cui, X. Xu, and W. Yao, Nat. Commun. **4** 2053 (2013).
- [18] X. Zhang, Q. Liu, J.-W. Luo, A. J. Freeman, and A. Zunger, Nat. Phys. **10**, 387 (2014).
- [19] G. Kresse and J. Furthmüller, Comp. Mater. Sci. **6**, 15 (1996).
- [20] G. Kresse and D. Joubert, Phys. Rev. B **59**, 1758 (1999).
- [21] See Supplementary Material at [URL] for the derivation of Eq. (6), three kinds of other relaxation channels, possible reasons for the deviation between theory and experiment and supplementary figures.
- [22] R. Suzuki *et al.*, Nat. Nanotech. **9**, 611 (2014).
- [23] J. M. Riley *et al.*, Nat. Phys. **advance online publication**. doi:10.1038/nphys3105 (2014).
- [24] L. Dong, A. M. Dongare, R. R. Namburu, apos, T. P. Regan, and M. Dubey, Applied Physics Letters **104** 043715 (2014).
- [25] We noted that the calculated circular polarization does not change if the MX₂ layers are slightly shifted or rotated relative to each other.
- [26] J. Klimeš, D. R. Bowler, and A. Michaelides, Phys. Rev. B **83**, 195131 (2011).
- [27] G.-H. Lee *et al.*, ACS Nano **7**, 7931 (2013).
- [28] C. L. Heideman, S. Tepfer, Q. Lin, R. Rostek, P. Zschack, M. D. Anderson, I. M. Anderson, and D. C. Johnson, J. Am. Chem. Soc. **135**, 11055 (2013).

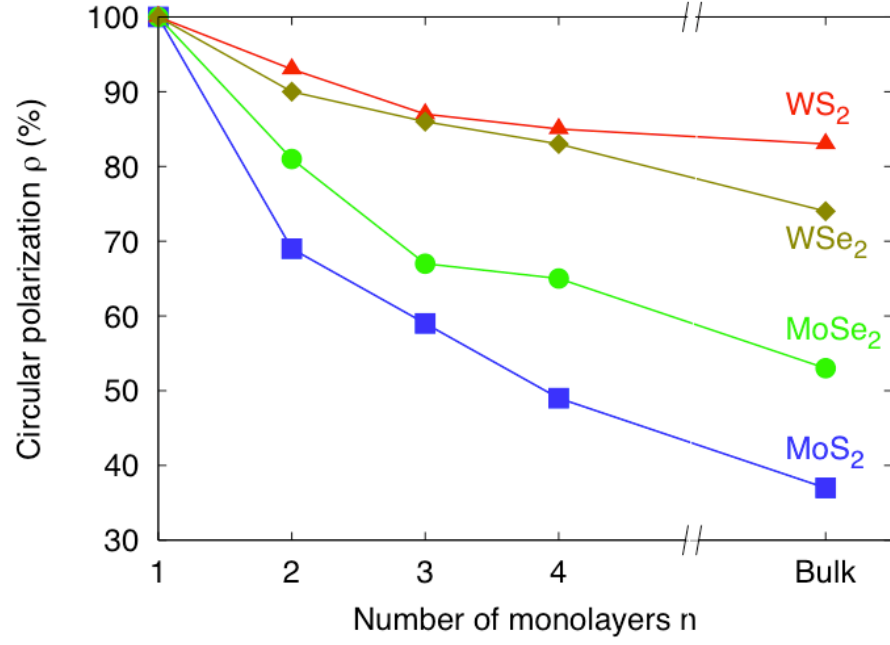


Fig. 1: Calculated circular polarization ρ from Eq. (6) of different $(MX_2)_n$ materials as a function of the number of monolayers n . We consider resonant excitation at K and $-K$ valley by circular polarized light. The values of σ_+ and σ_- excitation have the same magnitude but opposite sign.

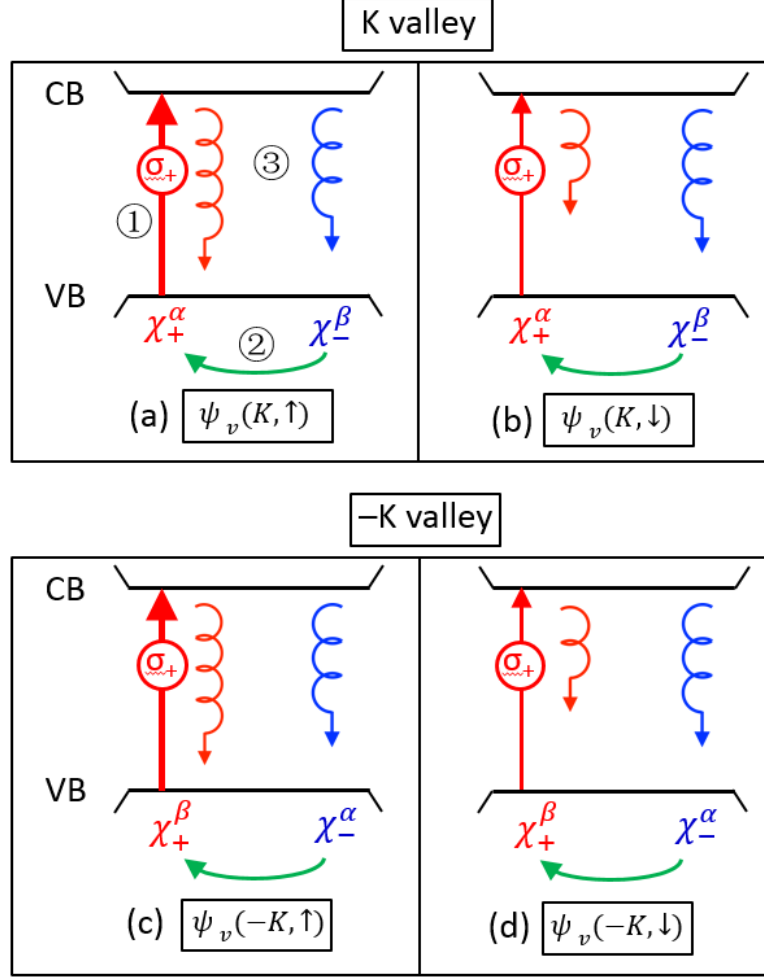


Fig. 2: Schematic diagram of photoluminescence process at K and $-K$ valley in bilayer MX_2 . Four degenerate valence band (VB) states described in Eq. (4) and (5), i.e., (a) $\psi_v(K, \downarrow)$, (b) $\psi_v(K, \uparrow)$, (c) $\psi_v(-K, \downarrow)$, and (d) $\psi_v(-K, \uparrow)$, are shown with χ_+ (red) and χ_- (blue) denoting LH and RH orbitals of the valence states, respectively. Taking panel (a) as an example, three steps in photoluminescence are indicated. ① Absorption by a resonant σ_+ excitation. The red arrow indicates that the excitation promotes electrons with χ_+ character into conduction band (CB). ② Intrastate relaxation denoted by green arrows. ③ Radiative recombination filling the holes of VB state. The red and blue curled arrows denote σ_+ and σ_- emission, respectively, with the lengths representing the relative intensity of emission regarding $C_{maj} > C_{min}$.

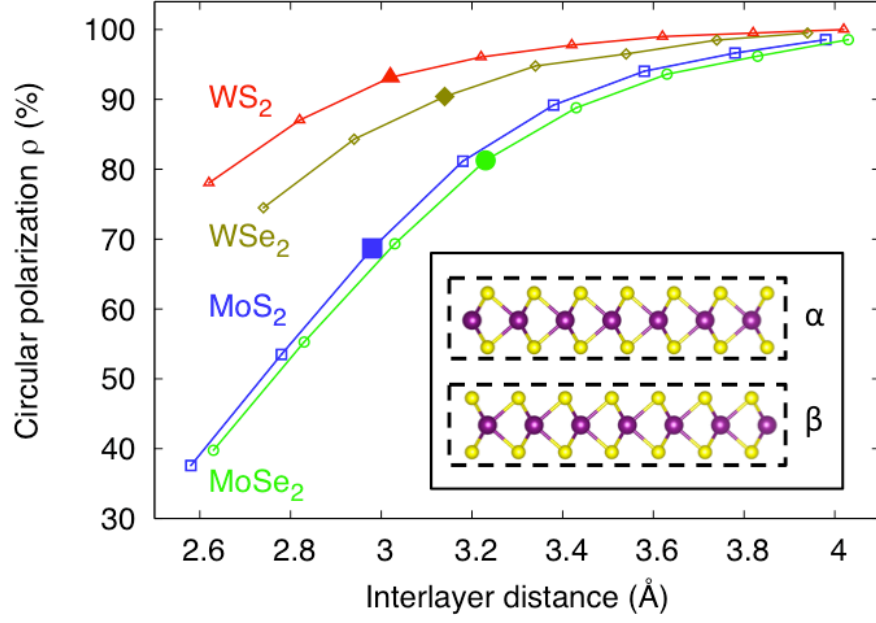


Fig. 3: The circular polarization ρ as a function of the interlayer distance of bilayer MX_2 materials. The larger solid symbols denote the experimental interlayer distance. The inset shows the crystal structure of bilayer MX_2 , with the purple and yellow balls denoting M and X atoms, respectively.